

Beam transmission of water-embedded steel plate at normal incidence. Diffraction effects in the S_1 to A_3 region

Magne Aanes^{a,b,c,*}, Kjetil Daae Lohne^{b,c}, Espen Storheim^{b,c},

Per Lunde^{a,b,c}, and Magne Vestrheim^{a,c}

^a University of Bergen, Department of Physics and Technology, P.O. Box 7803, N-5020 Bergen, Norway

^b Christian Michelsen Research AS (CMR), P.O. Box 6031 Postterminalen, N-5892 Bergen, Norway

^c The Michelsen Centre for Industrial Measurement Science and Technology

Abstract

Measurement of the sound transmission through a fluid-embedded viscoelastic plate at normal incidence can show significant deviations to the plane-wave theory, experiencing both frequency shift and signal level variation in relation to the plane-wave theory. These deviations become important when relating measurements to e.g. cut-off frequencies in the plane-wave theory to determine material parameters of the plate. Models developed, which incorporate a more realistic 3D diffracted piezoelectric transducer beam, explains these phenomena, and using these tools the underlying physics can be studied.

1. Introduction

Sound propagation in viscoelastic fluid-embedded plates has been a subject of extensive research. The topic is of interest for several applications, e.g. non-invasive ultrasonic flow metering, pipeline deposit detection, non-destructive testing and wall-thickness monitoring. The plane-wave theory for fluid-embedded viscoelastic plates, e.g. [1,2], is often used in such waveguide applications to estimate either the wall thickness or sound velocities [3,4,5] of the plate or pipe wall. In normal incidence through-transmission measurements, a frequency shift associated with the excitation of certain leaky Lamb modes (guided waves), and an associated increased transmission, in relation to the plane-wave theory, has been observed by e.g. [3,5,6,7,8,9,10]. It has been shown that for relevant transducer dimensions and frequencies, a plane-wave approach is not sufficient for accurate description of guided waves in the solid plate and the associated leaky sound waves in the surrounding fluid, e.g. [3,6,7,8,9,10,11]. Attempts have been proposed to minimize these deviations, amongst other by approximating a plane wave using either large transducers [3], or using spatial-weighted measurements [4].

Models developed in [7,9,11], incorporate a realistic bounded beam from a finite dimensional piezoelectric transducer and its vibration, including the electro-acoustical coupling, and its interaction with a fluid-embedded viscoelastic plate. This includes the excitation of leaky Lamb modes in the plate, and the 3D diffracted sound pressure transmitted through the plate. Since use of a commercial transducer does not provide sufficient information regarding the transducer construction, dimensions and materials involved, a piezoelectric transducer has been designed, constructed, characterized and used for measurements and finite element (FE) simulations. This includes a more realistic transducer/beam description than e.g. the baffled piston model or Gaussian sources [7]. By including the piezoelectric transducer in the theoretical description of the measurement system, a quantitative (absolute scale) description of the signal chain, from electrical voltage into the transducer – to the transmitted pressure through the plate is accomplished. The 3D signal propagation in both time and frequency domain (including signal waveforms, signal spectra, and transfer functions), and

*) Corresponding author, email address: magne.aanes@ift.uib.no (Magne Aanes)

transducer fields, have been successfully compared to measurements. Axisymmetric finite elements are used to simulate the signal propagation through this measurement system at normal beam incidence, denoted the FEM approach. This approach is extended to account for an arbitrary angle of incidence using a hybrid approach, involving finite element modeling combined with an angular spectrum method (ASM), denoted the hybrid FEM-ASM approach. In this approach the transducer's voltage-to-pressure response and free-field sound pressure is calculated using FEM. This FEM simulated sound pressure field is further propagated through the plate and the surrounding fluid using the ASM and the exact plane-wave pressure transmission coefficient.

In the present work, these models are used to investigate in close detail the discrepancies between measurements and the plane-wave theory. More specifically, the discrepancies at normal incidence (frequency shift and signal level variation) located in the S_1 to A_3 (leaky Lamb modes) region. A case study is presented to investigate these discrepancies in relation to the longitudinal and shear velocities in the plate, i.e. the proximity of the cut-off frequencies for the leaky Lamb modes at normal incidence. The aim is to investigate possible connections between the frequency shift and the proximity of leaky Lamb modes with similar symmetry, and between the signal level variation and the sign of the group velocity of the excited mode.

2. Theory

Fig 1 shows an illustration of a measurement system consisting of a piezoelectric transducer radiating in water towards a steel plate, at normal beam incidence. An electrical signal V_0 is generated by a signal generator and fed to the piezoelectric transducer, which experiences a voltage V due to the generator's internal impedance Z_0 . The signal is then propagated through the transducer and into the surrounding water, and transmitted through the steel plate, being detected by a hydrophone at a given receiver position, marked * in Fig. 1. A 3D Cartesian coordinate system is used to describe the sound propagation through this system, where the z -axis is chosen orthogonal to the plate and directed downwards, and the plate is in the xy -plane, at distance $z = z_0$ (upper surface), the plate thickness is $t = 2L$ (where L is the half-thickness) and $z_1 = z_0 + 2L$ (lower surface). The signal propagation through the steel plate and subsequent fluid region is governed by the pressure-to-pressure transfer function given as [7]

$$H_{PP}(x, y, z_2, f) = \frac{P_t(x, y, z_2, f)}{P_0(0, 0, z_0, f)} \quad (1)$$

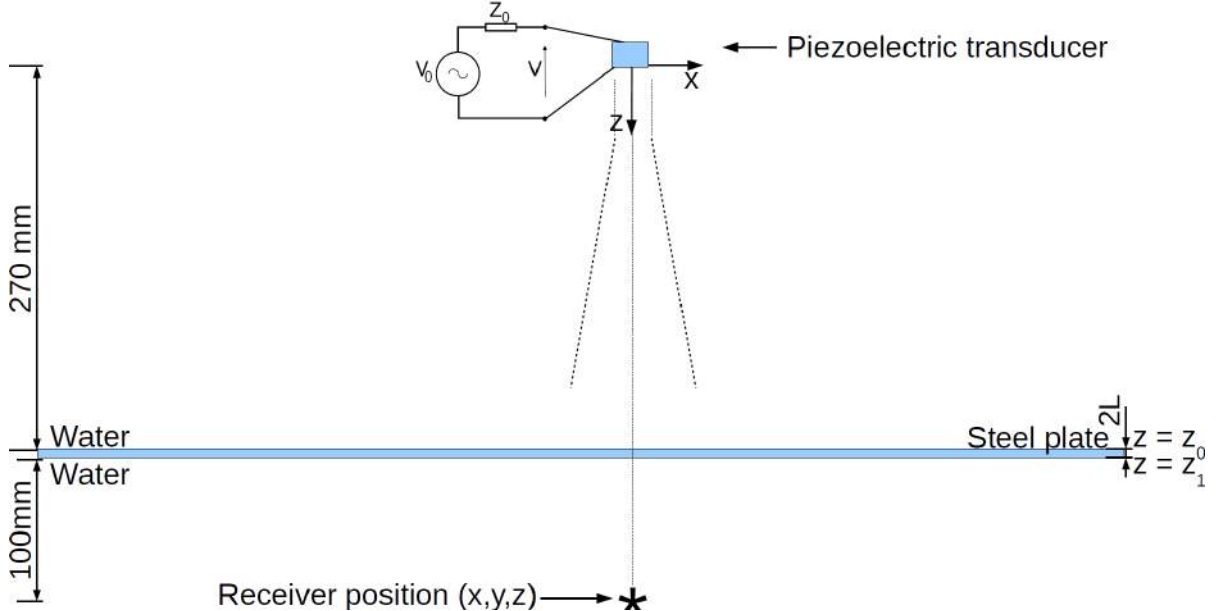


Fig 1: An illustration of the system consisting of a piezoelectric transducer, generating an acoustic beam at normal beam incidence towards a water-embedded viscoelastic steel plate. y is directed out of the paper.

where $P_t(x, y, z_2, f)$ is the transmitted free-field sound pressure spectrum, at the hydrophone depth z_2 , and $P_0(0, 0, z_0, f)$ is the incident axial free-field sound pressure spectrum at the upper surface of the steel plate. f is the frequency. This transfer function can be decomposed as

$$H_{PP}(x, y, z_2, f) = H_{PP}^{plate}(x, y, z_1, f)H_{PP}^{prop}(x, y, z_2, f), \quad (2)$$

where

$$H_{PP}^{plate}(x, y, z_1, f) = \frac{P_1(x, y, z_1, f)}{P_0(0, 0, z_0, f)}, \quad (3)$$

and

$$H_{PP}^{prop}(x, y, z_2, f) = \frac{P_t(x, y, z_2, f)}{P_1(x, y, z_1, f)}. \quad (4)$$

$P_1(x, y, z_1, f)$ is the transmitted sound pressure spectrum at the lower surface of the plate. $H_{PP}^{plate}(x, y, z_1, f)$ governs the signal transmission through the steel plate, and $H_{PP}^{prop}(x, y, z_2, f)$ governs the sound transmission from the lower surface of the steel plate to the receiver depth, z_2 .

In the frequency-wavenumber domain, the plane-wave pressure transmission coefficient $T(h_{f,x}, h_{f,y}, L, f)$ for the steel plate is given as [4,7]

$$T(h_{f,x}, h_{f,y}, L, f) = \frac{P_1(h_{f,x}, h_{f,y}, z_1, f)}{P_0(h_{f,x}, h_{f,y}, z_0, f)} = \frac{-iY(A + S)}{(S + iY)(A - iY)}, \quad (5)$$

where $h_{f,x}$ and $h_{f,y}$ are the compressional horizontal wavenumbers in the x - and y -directions, respectively. $P_0(h_{f,x}, h_{f,y}, z_0, f)$ is the axial incident free-field frequency-wavenumber spectrum in the water at $z = z_0$. $P_1(h_{f,x}, h_{f,y}, z_1, f)$ is the transmitted frequency-wavenumber spectrum at $z = z_1$. S, A, Y are the terms associated with the symmetrical and anti-symmetrical Lamb modes (guided waves), and the fluid loading in the plate given in Eqs. (2.49), (2.50) and (2.91) in [7]. Note that $H_{PP}^{plate}(x, y, z_1, f)$ is defined in the frequency-spatial domain, whereas $T(h_{f,x}, h_{f,y}, L, f)$ is defined in the frequency-wavenumber domain.

3. Measurements

It is referred to [7] for details on the measurement setup.

4. Simulations

The hybrid FEM-ASM approach is used to calculate the transmitted sound pressure at the receiver depth z_2 , at normal beam incidence. FEM is used to calculate the free field sound pressure from the piezoelectric transducer at $z = z_0$. Interpolation is used to fit data (from the fluid FE nodes) onto an ASM grid. ASM is used to transform this incident pressure into the wavenumber-frequency domain by a 2D spatial Fourier transform in the (x, y) -plane, and propagate this sound field through the plate using the plane-wave pressure transmission coefficient given in Eq. (5). The plane wave propagator [7] is then used to propagate it further to the receiver depth z_2 , before calculating the transmitted sound pressure in the frequency-spatial domain by a 2D inverse spatial Fourier transform. For more detail and description of the hybrid FEM-ASM, and the FEM approach, it is referred to [7,11].

For our case study, the following sound velocities for the steel plate are used:

- Case 1) the longitudinal sound velocity c_L is 5780 m/s, the shear velocity c_S is 3130 m/s.
- Case 2) c_L is 5780 m/s and c_S is 3900 m/s.

Information regarding the rest of the material parameters of the plate, and the surrounding water is given in [7]. The dispersion curves and group velocities of the plates are calculated using MODEST [12]. The finite element model used in this work is the FEMP 5.0 program [13,14].

5. Results

5.1. Models compared to measurements at normal beam incidence (case 1)

In Fig. 2 the magnitude of the plane-wave pressure transmission coefficient $|T(h_{f,x}, h_{f,y}, L, f)|$ for the steel plate with material parameters from case 1 is shown as a function of plane-wave incidence angle θ (in the range $0-60^\circ$) and frequency, calculated using Eq. (5). S and A denote symmetrical and anti-symmetrical leaky Lamb modes in the plate, respectively. The zeroth order symmetrical and anti-symmetrical modes are defined as S_0 and A_0 , respectively. The S_1, A_1, S_2, A_2 and A_3 modes are defined in ascending order in relation to their corresponding cut-off frequency, and are defined from case 1 and used throughout this paper. As the plane-wave angle of incidence approaches zero, the symmetrical and anti-symmetrical leaky Lamb modes in the plate

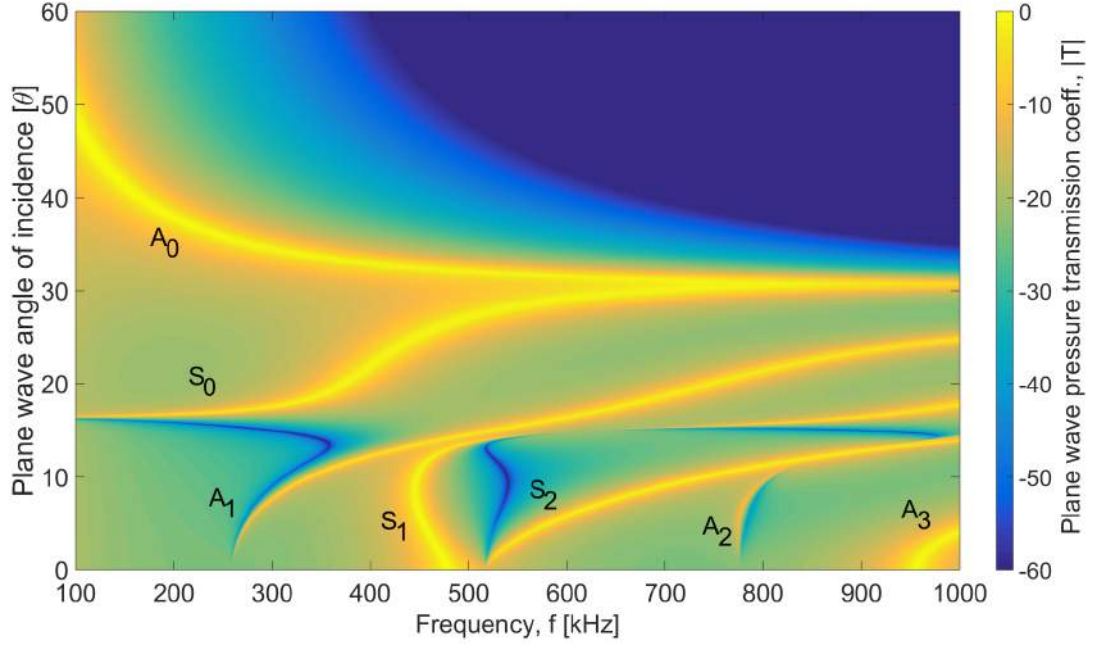


Fig 2: Magnitude of the plane-wave pressure transmission coefficient $|T(\mathbf{h}_{f,x}, \mathbf{h}_{f,y}, L, f)|$, as a function of plane-wave angle of incidence and frequency, including leaky Lamb modes in the water-embedded steel plate. The material data is taken from case 1.

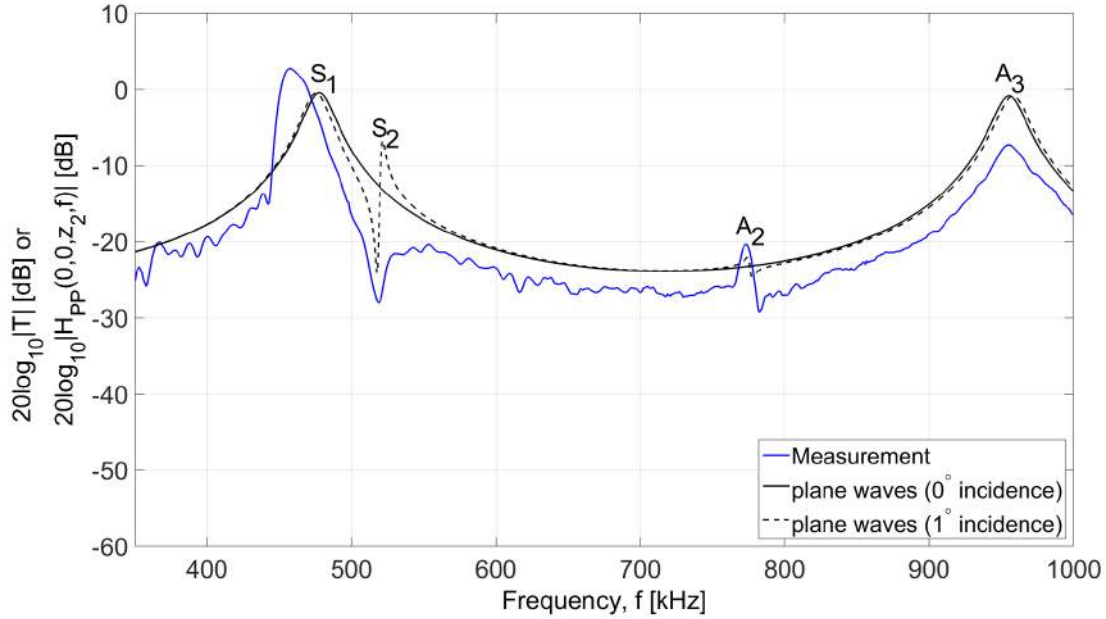


Fig 3: The magnitude of the plane-wave pressure transmission coefficient $|T(\mathbf{h}_{f,x}, \mathbf{h}_{f,y}, L, f)|$, for plane wave incidence angle θ of 0° and 1° (black lines), in comparison with the measured pressure-to-pressure transfer function $|H_{PP}(x, 0, z_2, f)|$ (blue line). The leaky Lamb modes in the plate are indicated at their respective frequencies.

approach the cut-off frequencies, creating standing waves (thickness-extensional (TE) and thickness-shear (TS) modes, respectively) across the thickness of the plate. Since a plane wave at normal incidence only generates compressional displacement in the plate, only modes associated with compressional waves appear inside the plate, exciting the S_1 and A_3 modes. For that reason a plane-wave at normal incidence cannot excite TS modes in the plate, and the leaky Lamb modes associated with these modes, the S_2 and A_2 modes, will vanish as θ approaches zero. For case 1, the frequencies corresponding to the leaky Lamb modes S_1 , S_2 , A_2 and A_3 for a normal incident plane wave cf. Fig. 2 are 477.7 kHz, 517.5* kHz, 774.5* kHz and 955.4 kHz respectively. The superscript * indicates that a plane wave at 1° incident angle has been used to calculate the corresponding

leaky Lamb mode. Fig 3 shows the measured (blue line) $|H_{PP}(0,0,z_2,f)|$ as a function of frequency, calculated using Eq. (1), in comparison to the plane-wave theory (using plane waves at 0° and 1° (black lines) incidence angles). The lower level of the measurements relative to the plane-wave theory (approx. 3 dB) originates from the fact that $|H_{PP}(0,0,z_2,f)|$ is measured at a distance of 100 mm from the plate, see Fig. 1. The discrepancies that is of interest in this investigation is that of the downwards frequency shift and signal level increase of the measured transmission associated with the S_1 mode excitation, and the smaller upwards frequency shift and signal level decrease of the measured transmission associated with the A_3 mode excitation, in relation to the plane-wave theory.

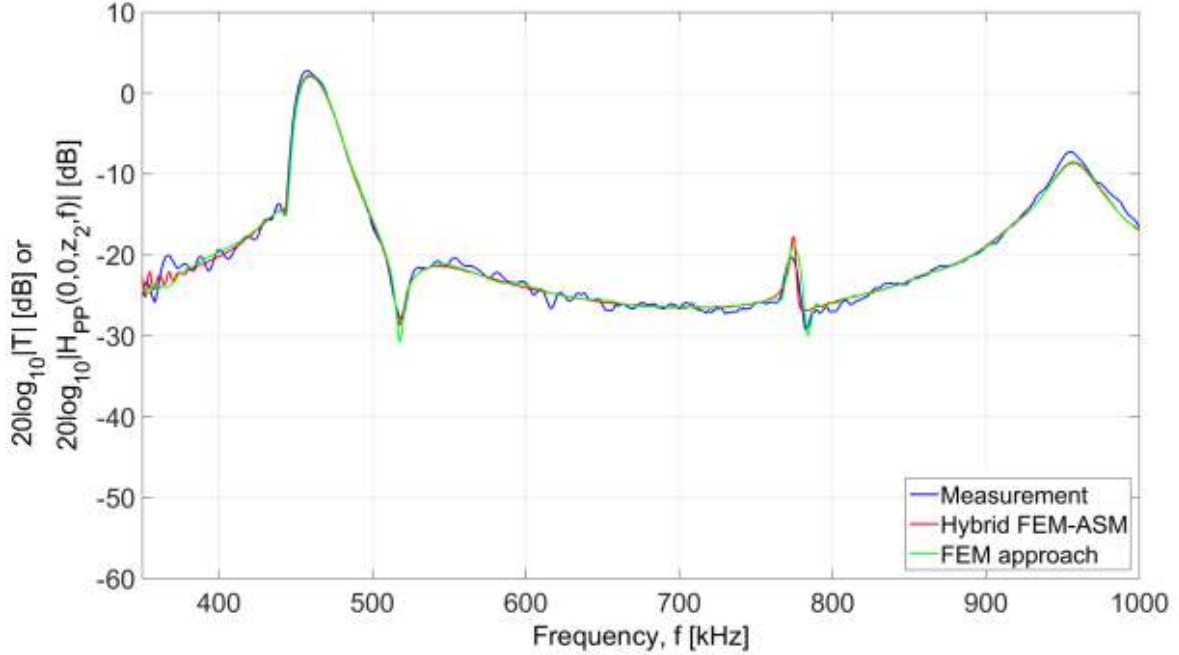


Fig 4: Simulated magnitude of the pressure-to-pressure transfer function $|H_{PP}(x, 0, z_2, f)|$ using the hybrid FEM-ASM (red line) and FEM approaches (green line), in comparison to measurements (blue line).

Fig 4 shows the measured $|H_{PP}(0,0,z_2,f)|$ as a function of frequency, in comparison to the simulated $|H_{PP}(0,0,z_2,f)|$ using the FEM and hybrid FEM-ASM approaches (green and red lines, respectively). Here, one can observe that the simulation models agree within 1.2 dB (not including the A_2 mode) with the measurements, also in terms of the frequency shift and signal level variation. Thus, both models seem to be capable of describing the measured results, and to investigate the discrepancies between the plane-wave theory and the experimental results.

5.2. Case 1: $c_L = 5780$ m/s, $c_S = 3130$ m/s

Fig 5 shows the simulated $|H_{PP}^{plate}(x,y,z_1,f)|$ using the hybrid FEM-ASM approach (green line), in comparison to the plane-wave pressure transmission coefficient $|T(h_{f,x}, h_{f,y}, L, f)|$ for plane waves at 0° (blue line) and 1° (red line) incidence angles. The hybrid FEM-ASM transmission associated with the S_1 mode is shifted downwards in frequency, and the signal level is increased above unity, in relation to the plane-wave theory. The hybrid FEM-ASM transmission around the A_3 mode has decreased in relation to the plane-wave theory, and experiencing minimal to no frequency shift.

In Fig 6 the dispersion curves for the leaky Lamb modes (blue lines) are shown as a function of frequency and plane-wave angle of incidence. The red line is the -3 dB angle of a uniformly vibrating plane piston mounted in a rigid baffle of infinite extent with radius equal to the effective radius of the piezoelectric transducer at $f = 575$ kHz [7], i.e. most of the beam energy is located below this line for a given frequency [7]. Within the -3 dB angle, the S_1 mode is excited at lower frequencies when increasing the plane-wave angle of incidence, while the A_3 mode is excited at higher frequencies. The S_1 and S_2 modes are relatively close in frequency at normal incidence, while the A_2 mode is further away in frequency to the A_3 mode.

In Fig 7 the group velocity for the leaky Lamb modes is shown as function of frequency. Note that the group

velocity is positive for all frequencies for the S_2 , A_2 and A_3 modes, while it is negative in a region for the S_1 mode.

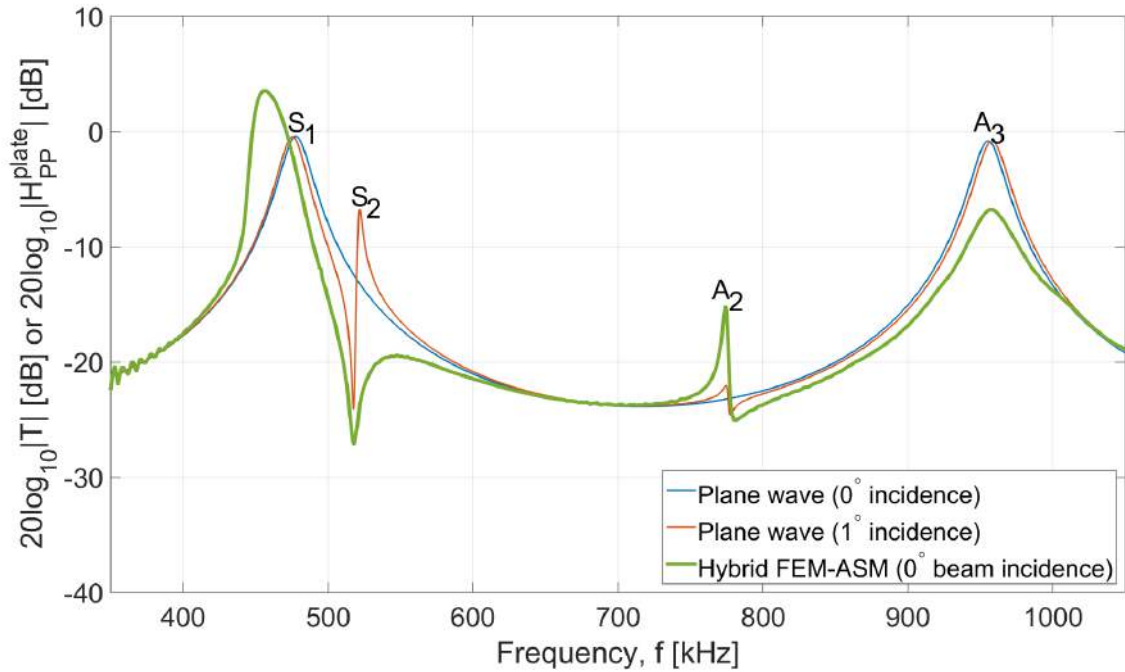


Fig 5: The magnitude of the plane-wave pressure transmission coefficient $|T(h_{f,x}, h_{f,y}, L, f)$ for plane waves at $\theta_p = 0^\circ$ (blue line) and 1° (red line) incidence angles, in comparison to H_{PP}^{plane} calculated using the hybrid FEM-ASM approach (green line). The leaky Lamb modes S_1 , S_2 , A_2 and A_3 are indicated at their respective frequencies. Case 1.

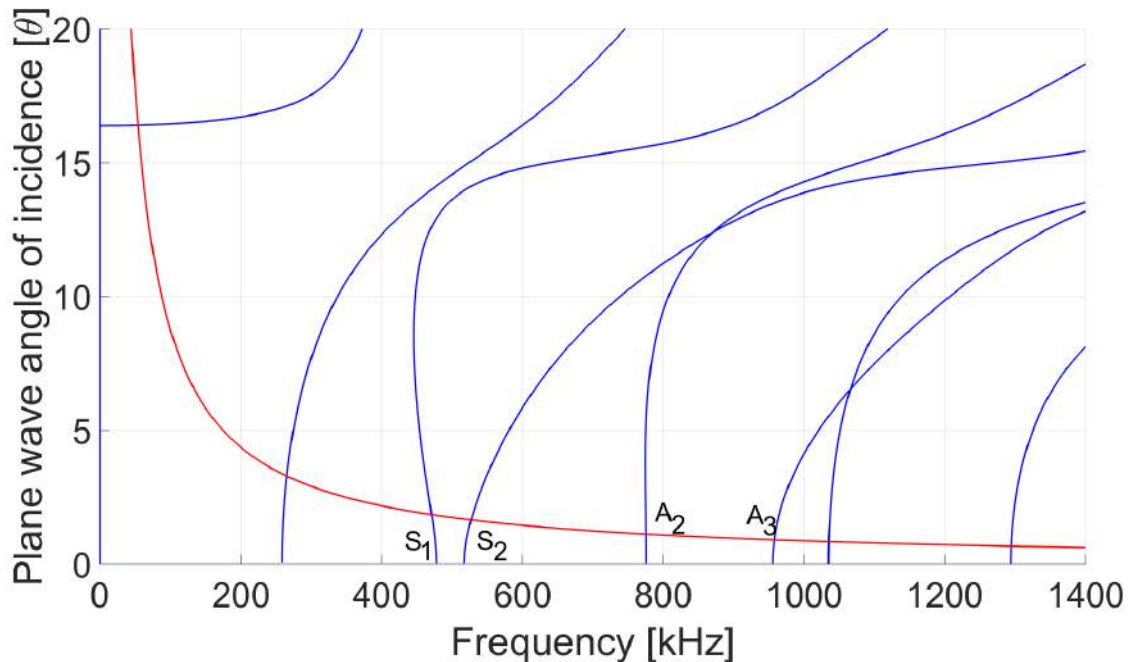


Fig 6: Dispersion curves for the leaky Lamb modes as a function of frequency and plane wave angle of incidence, θ . Case 1.

Fig 8 a) and b) show the simulated magnitude of the pressure field distribution in the (x, z) –plane when the piezoelectric source transducer is excited using $V = 1V$, near the leaky Lamb modes S_1 and A_3 , respectively. The incident pressure field is propagated from the piezoelectric transducer towards the steel plate, and the transmitted pressure field through the plate is calculated. The reflected field is omitted from the figures. At $f = 457$ kHz (transmission is associated with the S_1 mode) one can observe a beam narrowing effect through the

steel plate, while at $f = 956$ kHz (transmission is associated with the A_3 mode) one can observe a beam widening effect.

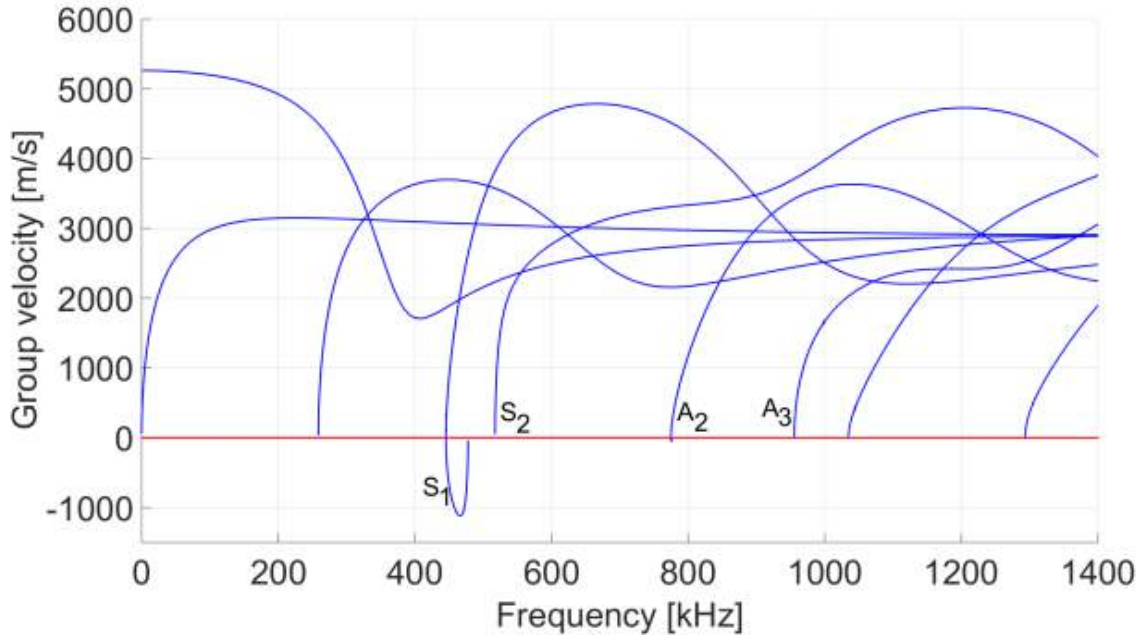


Fig 7: Group velocity for the leaky Lamb modes as a function of frequency. Case 1.

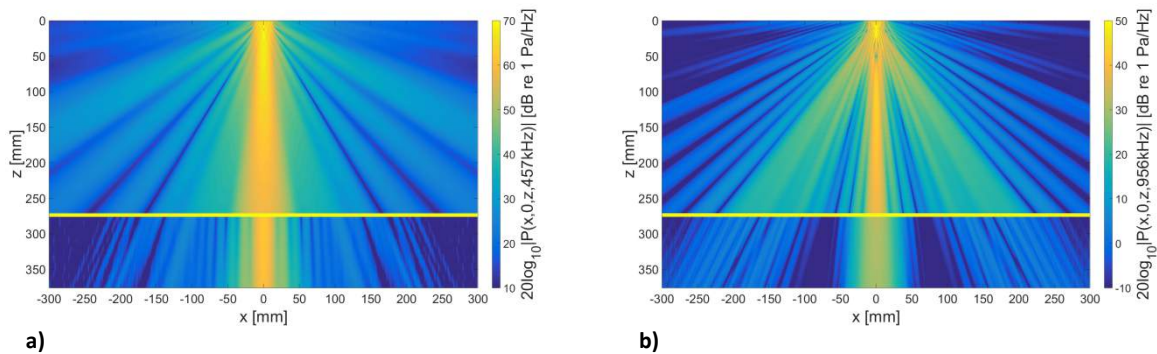


Fig 8: Simulated magnitude of the transducer radiated pressure field distribution $|P(x, 0, z, f)|$ using the hybrid FEM-ASM approach, a) at $f = 457$ kHz (near the S_1 mode) and b) at $f = 956$ kHz (near the A_3 mode). Case 1.

5.3. Case 2: $c_t = 5780$ m/s, $c_s = 3900$ m/s

Fig 9 shows the simulated $|H_{PP}^{plate}(x, y, z_1, f)|$ using the hybrid FEM-ASM approach (green line), in comparison to the plane-wave pressure transmission coefficient $|T(h_{f,x}, h_{f,y}, L, f)|$ for plane waves at 0° (blue line) and 1° (red line) incidence angles. The frequencies corresponding to the leaky Lamb modes S_1 , S_2 , A_3 and A_2 for a normal plane wave incident angle are 477.7 kHz, 648.1* kHz, 955.4 kHz and 983.0* kHz respectively. The superscript * indicates a 1° incidence angle with the plate. The hybrid FEM-ASM transmission associated with the S_1 mode experiences now a decreased frequency shift in relation to case 1, but still a frequency shift in relation to the plane-wave theory. The signal level is still above unity as for case 1. The hybrid FEM-ASM transmission associated with the A_3 mode experiences now a downward frequency shift and signal level increase in relation to the hybrid FEM-ASM transmission associated with the A_3 mode for case 1.

In Fig 10 the dispersion curves for the leaky Lamb modes (blue lines) are shown as a function of frequency and plane-wave angle of incidence. As an effect of the increased shear velocity the S_2 and A_2 modes are now moved upwards in frequency. The S_2 mode is now further away from the S_1 mode than in case 1, and the A_2 mode is now positioned at a higher frequency than the A_3 mode, and closer to the A_3 mode in relation to case 1. Observe that the S_1 is now excited at approximately the same frequency for low angles of incidence, in relation

to moving downwards in frequency for the same region in case 1. Observe further that the A_2 and A_3 modes are now relatively closer in frequency in relation to case 1. Now, the A_3 mode (within the -3 dB angle) is excited at lower frequencies when increasing the plane-wave angle of incidence. In Fig 11 the group velocity of the leaky Lamb modes is shown as a function of frequency. Note that the group velocity is now negative within a region for the A_3 mode, while the region with negative group velocity for the S_1 mode has decreased compared to case 1.

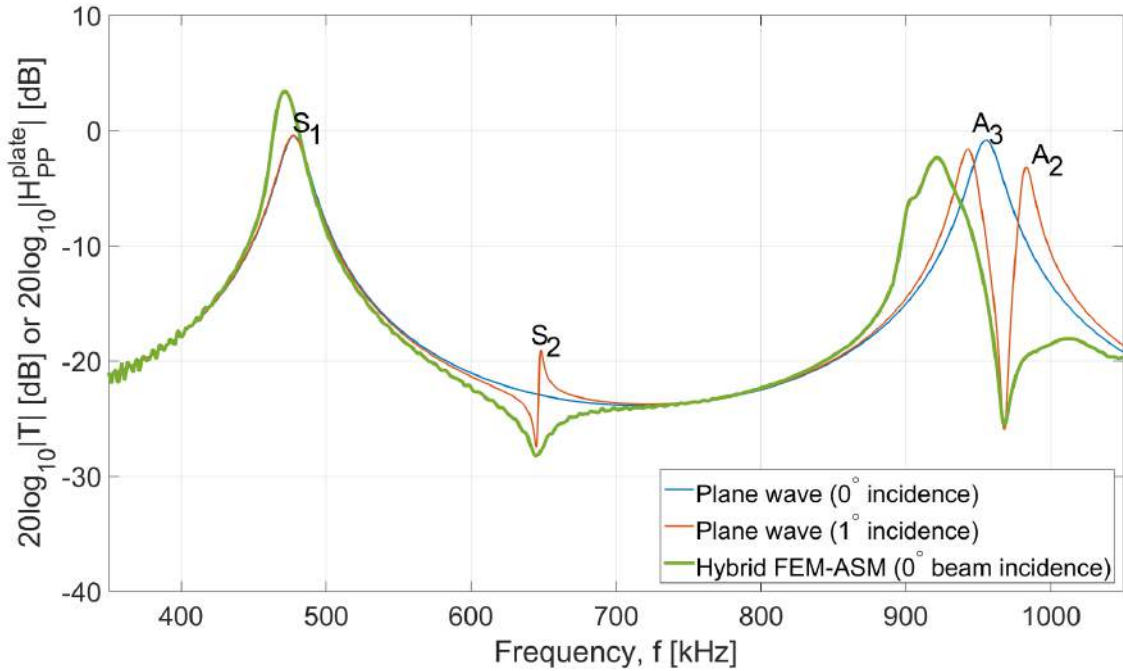


Fig 9: The magnitude of the plane-wave pressure transmission coefficient $|T(\mathbf{h}_{f,x}, \mathbf{h}_{f,y}, L, f)|$, for plane waves at $\theta_p = 0^\circ$ (blue line) and 1° (red line) incidence angles, in comparison to H_{pp}^{plane} calculated using the hybrid FEM-ASM approach (green line). The leaky Lamb modes S_1 , S_2 , A_2 and A_3 are indicated at their respective frequencies. Case 2.

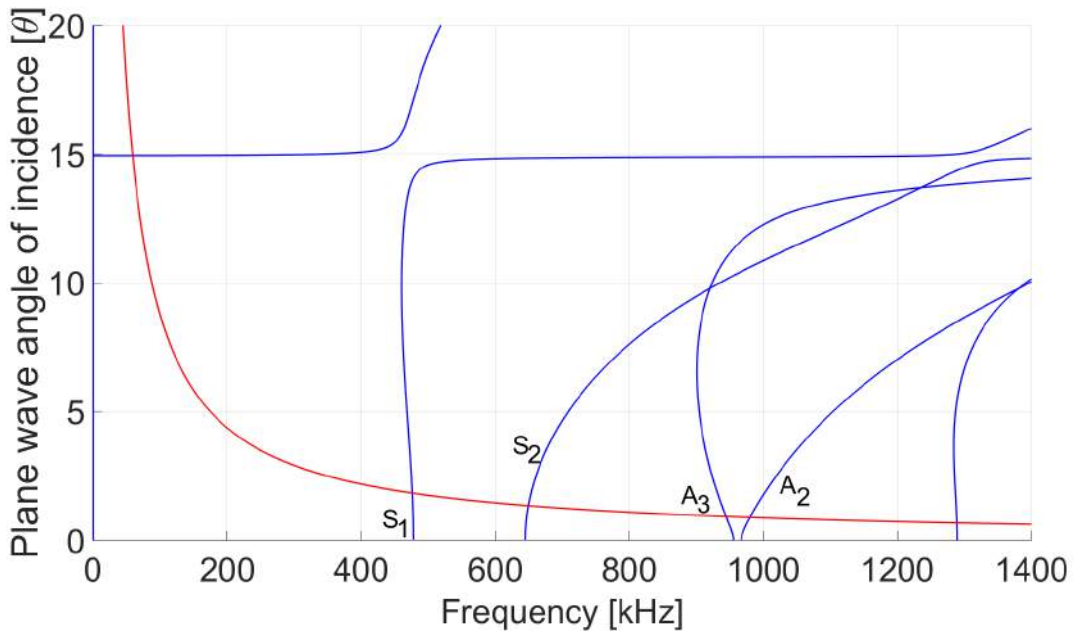


Fig 10: Dispersion curves for the leaky Lamb modes as a function of frequency and plane wave angle of incidence, θ . Case 2.

Fig 12 a) and b) show the magnitude of the pressure field distribution similar to Fig 8, near the leaky Lamb modes S_1 and A_3 . At $f = 471$ kHz (transmission is associated with the S_1 mode) one can observe a beam

narrowing effect, but it is less than for case 1 in Fig 8a). At $f = 924$ kHz (transmission is associated with the A_3 mode) one can observe a beam narrowing effect, in contrast to Fig 8b) for case 1, where the beam widened.

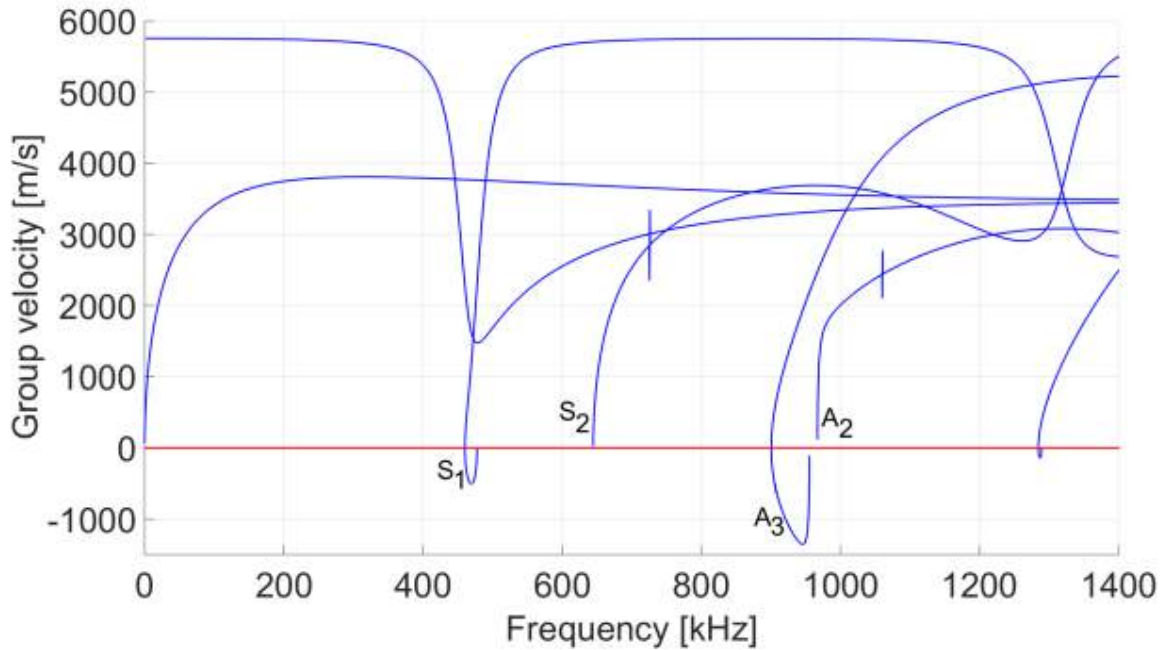


Fig 11: Group velocity for the leaky Lamb modes as a function of frequency. Case 2.

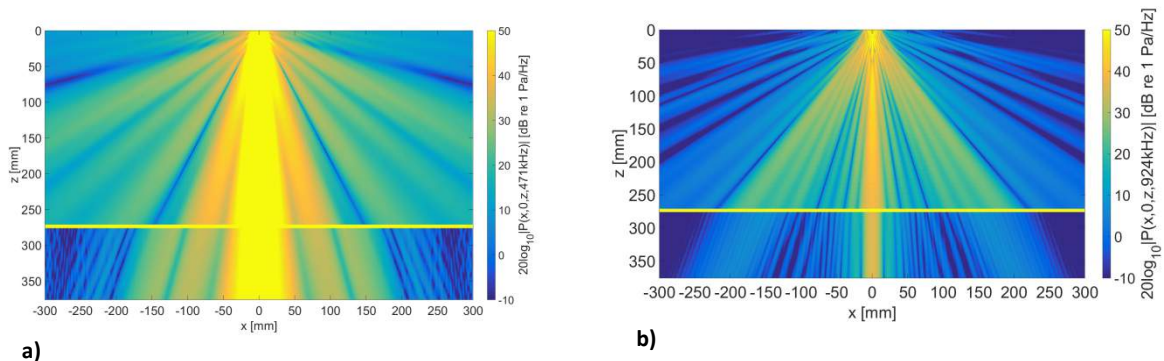


Fig 12: Simulated magnitude of the transducer radiated pressure field distribution $|P(x, 0, z, f)|$ using the hybrid FEM-ASM approach, a) at $f = 471$ kHz (near the S_1 mode) and b) at $f = 924$ kHz (near the A_3 mode). Case 2.

6. Conclusions

An investigation into the frequency shift and signal level variation experienced between the measured sound transmission through a water-embedded plate at normal incidence and the plane-wave theory has been undertaken. The hybrid FEM-ASM approach has been used to study the frequency shift and signal level variation comparing $H_{PP}^{plate}(x, y, z_1, f)$ and $T(h_{f,x}, h_{f,y}, L, f)$ in a case study. In the cases presented here a frequency shift is observed in relation to how close in frequency modes of similar symmetry are situated. With regard to the signal level variation, in the cases presented here, it is observed in relation to a mode having a negative group velocity.

Acknowledgements

Part of this work has been done under a PhD study financed by the University of Bergen, in a cooperation with Tor Arne Johansen, Department of Earth Science, UiB.

References

- ¹ H. Reissner, "Der senkrechte und schräge Durchtritt einer in einem flüssigen Medium erzeugten ebenen Dilatations Welle durch eine in diesem Medium befindliche plan-parallele feste Platte", *Helvetica Physics Acta*, vol. 11, pp. 408 – 431, 1938.
- ² M.F.M. Osborne and S.D. Hart, "Transmission, reflection and guiding of an exponential pulse by a steel plate in water. 1. Theory", *Journal of the Acoustical Society of America*, vol. 17, pp. 1 – 18, 1945.
- ³ P. Cawley and B. Hosten, "The use of large ultrasonic transducers to improve transmission coefficient measurements on viscoelastic anisotropic plates", *Journal of the Acoustical Society of America*, vol. 101, pp. 1373 – 1379, 1997.
- ⁴ J. Jocker and D. Smeulders, "Minimization of finite beam effects in the determination of reflection and transmission coefficients of an elastic layer", *Ultrasonics*, vol. 46, pp. 42 – 50, 2007.
- ⁵ G. Waag, L. Hoff and P. Norli, "Air-coupled ultrasonic through-transmission thickness measurements", *Ultrasonics*, vol. 56, pp. 332- 339, 2015.
- ⁶ K.D. Lohne, P. Lunde and M. Vestrheim, "Measurements and 3D simulations of ultrasonic directive beam transmission through a water-immersed steel plate", in *Proceedings of the 34th Scandinavian Symposium on Physical Acoustics*, Geilo, Norway, 30th January – 2nd February, 2011.
- ⁷ M. Aanes, "Interaction of piezoelectric transducer excited ultrasonic pulsed beams with a fluid-embedded viscoelastic plate", Ph.D. thesis, Department of Physics and Technology, University of Bergen, Bergen, Norway, 2013.
- ⁸ M. Aanes, P. Lunde and M. Vestrheim, "Ultrasonic beam transmission through a steel plate at oblique incidence. Uniform piston vs. piezoelectric transducer", in *Proceedings at the 36th Scandinavian Symposium on Physical Acoustics*, Geilo, Norway, 3rd – 6th February 2013.
- ⁹ M. Aanes, K.D. Lohne, P. Lunde and M. Vestrheim, "Normal incidence ultrasonic beam transmission through a water-immersed plate using a piezoelectric transducer. Finite element modeling, angular spectrum modeling and measurements", in *Proceedings of the International Congress on Sound Vibration*, Vilnius, Lithuania, 8th-12th July, 2012.
- ¹⁰ M. Aanes, K.D. Lohne, P. Lunde and M. Vestrheim, "Transducer beam diffraction effects in sound transmission of water-embedded steel plate, at normal incidence", Presentation given at the 37th Scandinavian Symposium on Physical Acoustics, Geilo, Norway, 2nd – 5th February, 2014.
- ¹¹ M. Aanes, K.D. Lohne, P. Lunde and M. Vestrheim, "Ultrasonic beam transmission through a water-immersed plate at oblique incidence using a piezoelectric source transducer. Finite element – angular spectrum modeling and measurements", in *IEEE International Ultrasonics Symposium Proceedings*, Dresden, Germany, 7th – 10th October, 2012.
- ¹² The MODEST-model was implemented by Remi A. Kippersund at Christian Michelsen Research AS, Bergen, Norway
- ¹³ J. Kocbach, "Finite element modeling of ultrasonic piezoelectric transducers", Ph.D thesis, Department of Physics, University of Bergen, Bergen, Norway, 2000.
- ¹⁴ J. Kocbach, P. Lunde, and M. Vestrheim, "Resonance frequency spectra with convergence tests of piezoceramic disks using the finite element method", *Acta Acustica*, vol. 87, pp. 271-285, 2001.